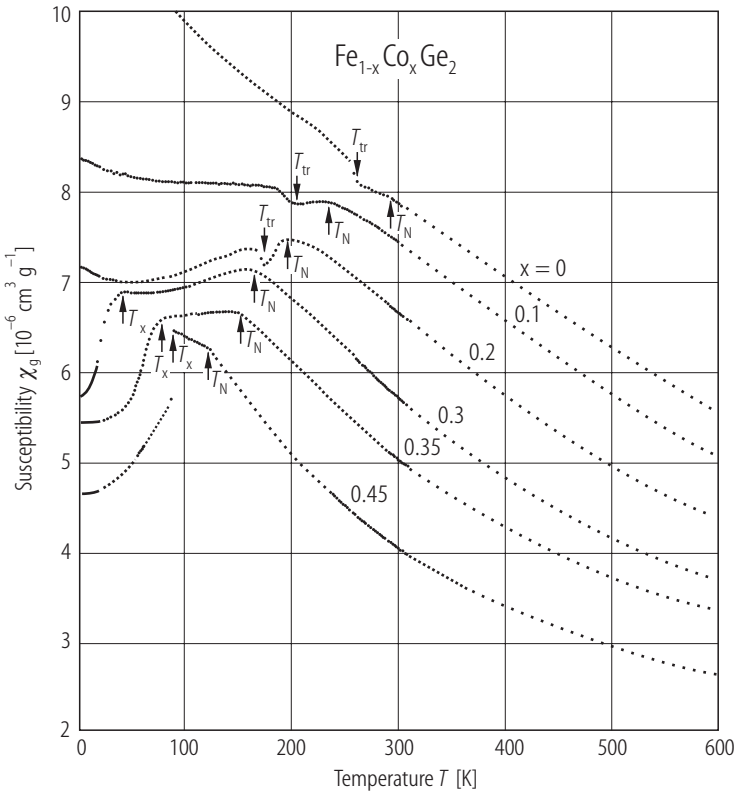

Fig. 105. $Fe_{1-x}Co_xGe_2$. Temperature dependence of the magnetic mass susceptibility χ_g in a magnetic field of 10 kOe. T_N: Néel temperature; T_{tr}: transition temperature to modulated spin structure; T_x: transition temperature of unknown origin [93S3].

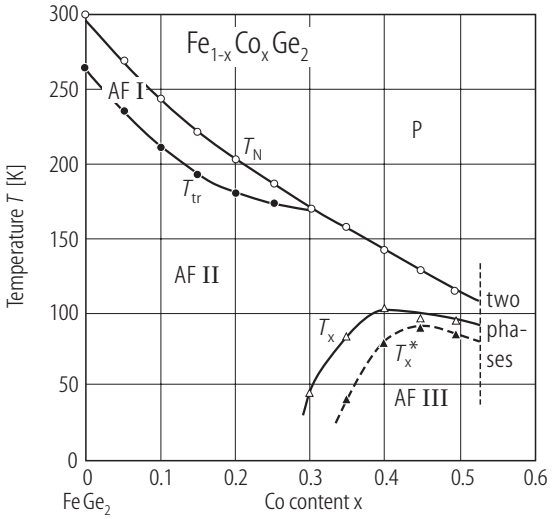

Fig. 106. $Fe_{1-x}Co_xGe_2$. Magnetic phase diagram in a composition - temperature plane, as obtained from magnetic measurements. AF I: antiferromagnet with modulated spin structure; AF II: with collinear structure; AF III: unknown structure. Magnetization curves of polycrystal specimens are linear below T_x^* and above T_{tr} [93S3].

1.5.4.5.3 Alloys and compounds with Sn

Magnetic structure of $FeSn_2$ has been re-investigated. Unfortunately, the single crystal specimen is very difficult to obtain, because $FeSn_2$ is formed through a peritectic reaction of FeSn and a Sn-rich liquid. The neutron-diffraction analysis has to be performed using powder specimens, leading to some ambiguity in the proposed magnetic structure.

Survey

	Properties	Figure	Table
$FeSn_2$	magnetic structure	107	10
	$H_{hyp}(T)$	108	

Table 10. Supplement to Table 11 in LB III/19C, subsect. 1.5.4.5.3. Magnetic and related properties of $FeSn_2$ [87V2].

	$FeSn_2$
Crystal structure	tetragonal C16 ($CuAl_2$)
a [Å]	6.537
c [Å]	5.316
Magnetism	antiferro
T_N [K]	378
p_{Fe} [μ_B/Fe]	1.70 at 5 K
structure	T < 93 K: non-collinear; p_{Fe} canted from [110], cf. Fig. 107b 93 K < T < T_N : collinear. Ferromagnetic (010) planes couple antiferromagnetically. $p_{Fe} \parallel$ [010] at T_N rotate in the (001) plane as T is lowered. cf. Fig. 107a
H_{hyp} (^{119}Sn) [kOe]	66.5 Sn1 4 Sn2 32.5 Sn3 at 4.2 K cf. Fig. 108
IS (^{119}Sn) [mm s^{-1}]	2.30 [1]) at 4.2 K

[1]) Relative to $BaSnO_3$ at RT.

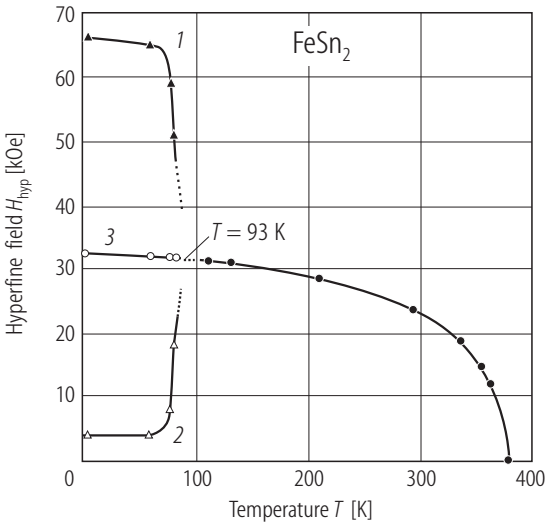

Fig. 108. $FeSn_2$. Temperature dependence of the hyperfine field H_{hyp} at an ^{119}Sn atom. The numerals *1*, *2*, and *3* correspond to B, A, and (C, C') Sn sites in Fig. 107b, respectively [87V2].

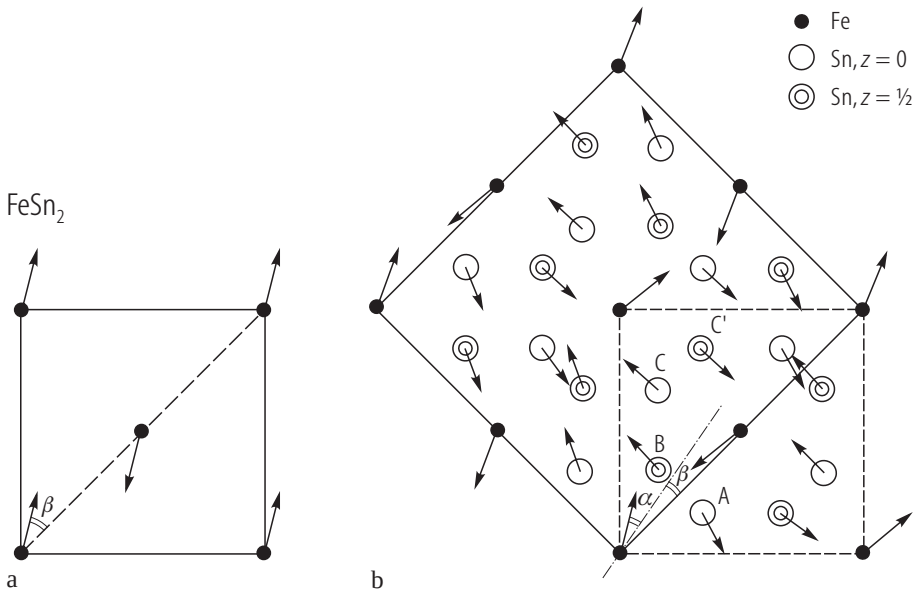

Fig. 107. $FeSn_2$. Antiferromagnetic structure proposed to explain both Mössbauer-spectroscopy [85L1, 87V2] and neutron- powder-diffraction [85V1] data. Projections onto tetragonal *c* plane. The Fe magnetic moments at *z* = 1/4 and 3/4 are parallel to each other and stay in the *c* plane. (**a**) Collinear structure between T_N = 378 K and T_{tr} = 93 K. The Fe moments, which are oriented along <100> (± [010] are chosen in the figure) at T_N (β = 45°), rotate continuously by 19° (β =26°) with decreasing temperature. (**b**) Noncollinear structure below T_{tr}. Hyperfine-field directions at Sn (at *z* = 0 and at *z* = 1/2) are also shown. Magnetic unit cell becomes twice as large as chemical cell: $a_{mag} = \sqrt{2}a$. From a line (in the ***c*** plane) which makes an angle β with $\boldsymbol{a}_{mag}$ ([110] of chemical cell), Fe moments deviate by α leading to a sequence of canting angles $\{\beta + \alpha, \pi + \beta - \alpha\}$ from ± $\boldsymbol{a}_{mag}$. With decreasing temperature, β decreases from 26° to ≈ 0° while α increases from 0° to 28° [87V2].

1.5.4.6 Co and Ni alloys and compounds

Antiferromagnetism is induced in a Co-Ge compound by Mn substitution.

Survey

	Composition x	Properties	Figure	Table
$Co_{7-x}Mn_xGe_6$	3.25	$\sigma(T)$, $\chi_g^{-1}(T)$	109	
	2.25...3.5	$T_N(x)$, $\Theta(x)$	110	
$CoGe_4$ [1])		a, χ_g		6

[1]) High-pressure synthesized compound.